Novel SiGe Island Coarsening Kinetics: Ostwald Ripening and Elastic Interactions

J. A. Floro* and M. B. Sinclair
Sandia National Laboratories, Albuquerque, New Mexico 87185-1415

E. Chason and L. B. Freund
Division of Engineering, Brown University, Providence, Rhode Island 02912

R. D. Twesten
Center for Microanalysis of Materials, University of Illinois, Urbana, Illinois 61801-2985

R. Q. Hwang
Sandia National Laboratories, Livermore, California 94551

G. A. Lucadamo
Department of Materials Science and Engineering, Lehigh University, Bethlehem, Pennsylvania 18015-3915
(Received 15 July 1999)

Real-time light scattering measurements of coherent island coarsening during SiGe/Si heteroepitaxy reveal unusual kinetics. In particular, the mean island volume increases superlinearly with time, while the areal density of islands decreases at a faster-than-linear rate. Neither observation is consistent with standard considerations of Ostwald ripening. Modification of the standard theory to incorporate the effect of elastic interactions in the growing island array reproduces the observed behavior.

PACS numbers: 68.35.Bs, 68.55.–a, 81.15.–z

Coherent island formation occurs to relieve strain associated with lattice mismatched heteroepitaxial growth [1–5]. Coherent islands have been shown to self-assemble to produce a narrow distribution of sizes, and to self-order spatially onto two- or three-dimensional lattices [6,7]. We have recently reported on the kinetics of self-ordering of [501]-faceted pyramidal islands ("hut clusters" [1]) in $Si_{0.8}Ge_{0.2}$ films on Si(001) during molecular beam epitaxy (MBE), where elastic repulsion between neighboring islands drives the spatial organization [8].

In this Letter we examine the kinetics of hut cluster coarsening during MBE growth, a process that is intimately associated with the self-ordering process. Coarsening is a competitive growth process wherein some islands grow at the expense of others in order to minimize total surface energy ("capillarity-driven coarsening"). The result is that the mean island volume increases with time, while the number of islands per unit area simultaneously decreases. Coarsening can occur via (i) Ostwald ripening [9,10], mediated by adatom diffusion currents between islands; (ii) dynamic coalescence, where islands themselves diffuse across a surface until they collide with other islands and coalesce into a single island [11]; and (iii) static coalescence, where islands do not translate but grow from supersaturation, undergoing coalescence only when neighboring islands touch [12]. We find that coarsening kinetics in dense arrays of hut clusters are much different than would be expected from simple capillarity-driven Ostwald ripening [9,10], even in the presence of a deposition flux. The novel kinetics observed here are attributed primarily to the effects of elastic interactions on Ostwald ripening. It is emphasized that only one type of island shape is present in these experiments, in contrast to previous studies [13–15].

$Si_{0.8}Ge_{0.2}$ films were grown on Si(001) by MBE (details may be found in [16]) at 755 °C and 0.1 Å/s deposition rate. Under these conditions, an extended regime of film thickness exists, from 60–130 Å mass equivalent thickness, in which {501}-faceted pyramidal islands are the only island morphology present [16]. Figure 1 shows an example of a typical hut cluster array, both as-deposited, and after annealing *in situ* at the growth temperature. As-deposited [Fig. 1(a)], the array is quite dense, with an areal coverage, defined as the fraction of substrate surface covered by islands, of $\theta = 0.7–0.8$. Coalescence of pyramids to form ridgelike structures is observed. After annealing at the growth temperature, the island array has coarsened further, and all islands are compact [501]-faceted pyramids.

In order to obtain the ensemble coarsening kinetics, the island array was characterized in real-time during MBE growth and annealing, using light scattering spectroscopy (LiSSp). LiSSp uses broadband illumination of the film surface, combined with spectroscopic detection of the scattered light, in a fixed scattering geometry [17]. For the lattice mismatch strain used here (0.8%), the island array is coarse enough to act as an optical diffraction grating [8,16]. From the peak in the scattered intensity we directly obtain the mean island spacing $\langle \lambda(t) \rangle$ and the mean areal density $\langle N(t) \rangle = \langle \lambda(t) \rangle^{-2}$ (number per area). The mean island volume is then given by $\langle V(t) \rangle = \langle \lambda(t) \rangle^2 [h_f(t) - h_{\mathrm{wl}}(t)]$, where h_f is the mass equivalent film thickness and h_{wl} is the wetting layer thickness. Cross-section transmission electron microscopy indicates that h_{wl} decreases slowly

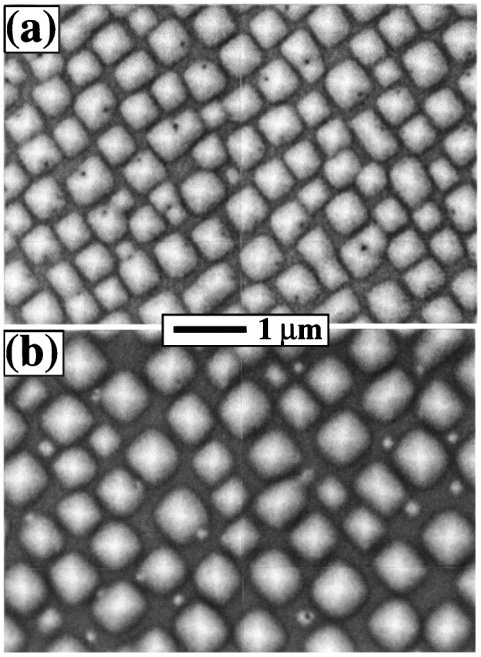

FIG. 1. Plan-view scanning electron micrographs of $Si_{0.8}Ge_{0.2}/Si(001)$ hut cluster arrays grown by MBE at 755 °C. (a) As-deposited (100 Å thick); (b) annealed for 40 min at the growth temperature (100 Å thick).

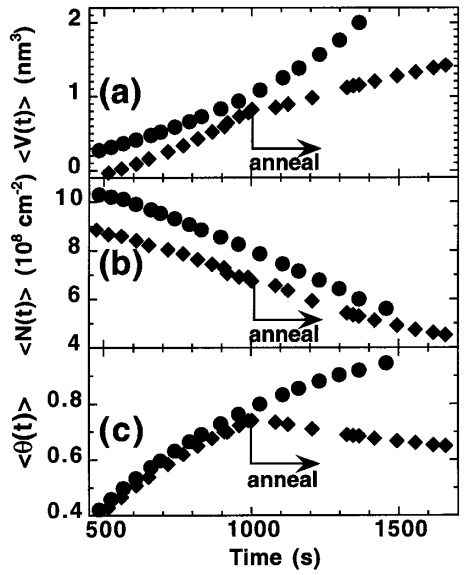

FIG. 2. LiSSp data obtained during growth of the films shown in Fig. 1. Circles are for continuous deposition, while diamonds are for deposition followed by annealing. In (a), the curves are offset for clarity.

during deposition during the hut cluster regime [18]. Since the time dependence is unknown, we have used a constant value of h_{wl} as a first approximation. The effect of this approximation will be discussed later. Finally, given the island shape, the mean areal coverage $\langle\theta(t)\rangle$ can also be calculated.

Figure 2 shows the LiSSp data obtained during deposition, and for deposition followed by annealing at the deposition temperature. The island array clearly coarsens during deposition, since $\langle V(t)\rangle$ increases while $\langle N(t)\rangle$ decreases (but the islands retain their {501}-faceted shape throughout). The areal coverage increases significantly during deposition but drops with annealing. The coarsening kinetics exhibit several unusual features of key importance here. First, for coarsening during deposition, $\langle V(t)\rangle$ increases *superlinearly* with time; that is, the second derivative is positive. A second key observation from Fig. 2 is that, during deposition, $d^2\langle N\rangle/dt^2$ is *negative*, which we show later is important in elucidating coarsening mechanisms. We also observe that the rate of coarsening during annealing is much slower than the coarsening during deposition, with $\langle V(t)\rangle$ increasing *sublinearly* with time and $d^2\langle N\rangle/dt^2$ is *positive*.

The coarsening kinetics we observe during deposition are inconsistent with elementary considerations of capillarity-driven Ostwald ripening, even in the presence of a deposition flux [10]. For deposition at constant rate, with no ripening, $\langle V(t)\rangle$ should increase linearly with time while $\langle N(t)\rangle$ remains constant. On the other hand, for Ostwald ripening with no deposition flux, $d^2\langle N\rangle/dt^2$ should always be positive. This is a consequence of the fact that as ripening proceeds, the driving force due to capillarity monotonically decreases with time, and the ripening rate decreases. To examine intermediate cases of ripening plus deposition, we employ a standard mean field analysis [13,19]. While such models cannot capture local behavior, we are interested here in the generic behavior of ensemble-average quantities, for which the mean field approach is reasonable. The chemical potential for pure capillarity-driven ripening is given by $\Delta\mu(V) = BV^{-1/3}$, where B sets the energy scale and V is an island volume (the Gibbs-Thomson equation). The growth rate of any class of islands of size V is, in the mean field context, given by [13]

$$\frac{dV}{dt} = cV^{1/3}[e^{\Delta\mu^*/kT} - e^{\Delta\mu(V)/kT}], \tag{1}$$

where c is a constant, kT is as usual, and $\Delta\mu^*$ is specified by conservation of mass:

$$\int_0^\infty f(V,t)\dot{V}\,dV = \Phi\,. \tag{2}$$

In Eq. (2), Φ is the deposition rate, $f(V,t)$ is the distribution of island volumes, and $\dot{V}$ is given by Eq. (1). Finally, the evolution of $f(V,t)$ is obtained from the flux continuity equation in size space,

$$\frac{\partial f}{\partial t} = -\frac{\partial(f\dot{V})}{\partial V}\,, \tag{3}$$

which is solved numerically [20]. From $f(V,t)$ we directly obtain $\langle V(t)\rangle$, $\langle N(t)\rangle$, and $\langle\theta(t)\rangle$ for comparison with data. The results are shown in Fig. 3. For pure ripening ($\Phi = 0$), $\langle V(t)\rangle$ increases linearly, $\langle N(t)\rangle$ decays with positive second derivative, and $\langle\theta(t)\rangle$ decreases, as expected, and is consistent with our postgrowth coarsening

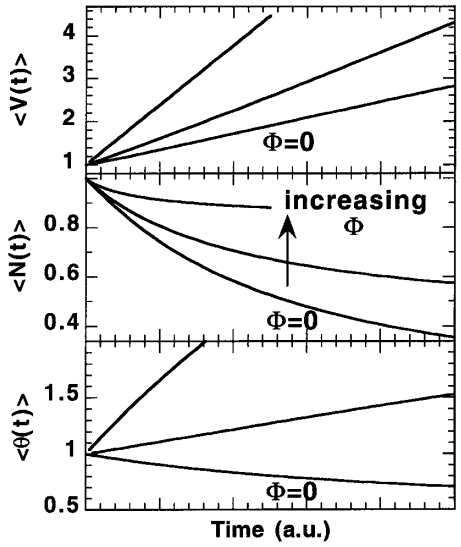

FIG. 3. Mean field model results showing effect of deposition flux, Φ. Note that $\langle N(t)\rangle$ always has positive second derivative, unlike the data shown in Fig. 2(b) for continuous deposition. $\langle V(t)\rangle$, $\langle N(t)\rangle$, and $\langle\theta(t)\rangle$ have been normalized by their initial values.

during annealing. For large Φ, where the deposition flux is much larger than the adatom supersaturation associated with ripening, $\langle V(t)\rangle$ again increases linearly with time, while $\langle N(t)\rangle$ decreases very slowly with time, again as expected. For intermediate Φ, $\langle N(t)\rangle$ still decays with positive curvature. Thus, capillarity-driven ripening, even in the presence of a deposition flux, cannot reproduce our essential experimental results.

We have shown previously that elastic interactions in dense arrays of hut clusters contribute significantly to the system energetics [8,20]. This should affect ripening, since during deposition, the increasing areal coverage of islands will continuously increase the elastic interaction energy. In essence, deposition combined with elastic interactions continuously drives the chemical potential of the island array upwards, forcing the system to respond by reducing the areal coverage through more rapid coarsening. The elastic interaction energy can be captured in the mean field approach to Ostwald ripening through an areal-coverage-dependent term in the chemical potential: $\Delta\mu(V,\theta) = B[V^{-1/3} + p(\theta)]$. In order to determine a form for $p(\theta)$, we performed finite element calculations of the elastic interaction energy as a function of areal coverage, using an axially symmetric configuration to capture the essence of the 3D situation (see Fig. 4 inset). The lateral faces of the cylindrical substrate are constrained against normal displacement to represent the symmetry constraint due to neighboring islands. The results are shown as circles in Fig. 4. We then fit the finite element results with $p(\theta) \propto \exp(\theta^2) - 1$, for use in the mean field model. This function is shown as the solid line in Fig. 4. The mean field areal coverage is explicitly evaluated at each time step and the analysis proceeds as described above.

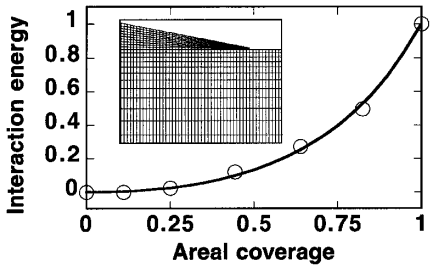

FIG. 4. Results of finite element calculations of the normalized excess elastic interaction energy as a function of areal coverage (circles). Also shown is an analytic representation (line). Inset: a 2D slice through the axisymmetric geometry used in the calculations.

Figure 5 shows results of calculations for $\langle V(t)\rangle$ and $\langle N(t)\rangle$ using a value of Φ such that coarsening is deposition dominated in the absence of elastic interactions (for comparison, the ripening kinetics for the same deposition rate but with no elastic interactions are also shown in the figure) [21]. The important outcome is that elastic interactions promote both superlinearity in $\langle V(t)\rangle$ and decay of $\langle N(t)\rangle$ with negative curvature. We also show our experimental data in Fig. 5 (open circles), scaled for comparison with calculations. A single scaling provides good generic agreement between the data and the mean field results. The quality of the agreement between model and experiment should not be overinterpreted—we seek only to demonstrate that the incorporation of elastic interactions in a simple Ostwald ripening model can reproduce the essential aspects of our experimental data.

In a previous study of coarsening by Ross *et al.* [13], ripening occurs within an island array consisting of both hut and dome clusters. Coarsening kinetics are dominated by the difference in chemical potential between domes and huts, which strongly drives dome growth at the expense of huts. Elastic interactions between islands in this case

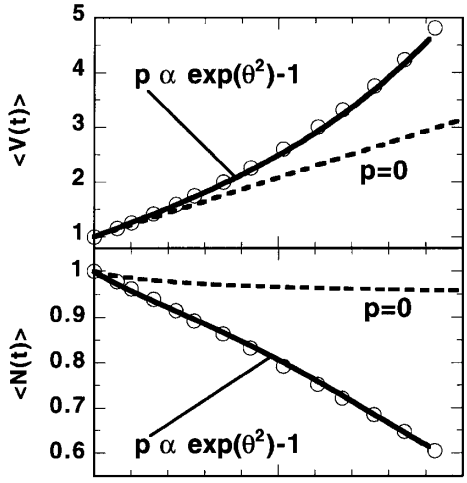

FIG. 5. Mean field model results incorporating elastic interactions at large Φ (solid line). Also shown for reference is $p(\theta) = 0$, i.e., no elastic interactions, but the same Φ (dashed line). The open circles are the data of Fig. 2, scaled for comparison.

might extend the hut—dome coexistence regime—since transforming to the higher aspect ratio domes decreases the local areal coverage. Our observations of island coarsening are not consistent with reports of stable, noncoarsening islands [22].

It is useful to consider other mechanisms that might contribute to our observed coarsening kinetics. For instance, we do not account for the small decrease in wetting layer thickness during the hut cluster regime and during annealing. However, we note that any time-dependent decrease of $h_{\mathrm{wl}}(t)$ does not affect our measured values for $\langle N(t)\rangle$ at all. Further, the wetting layer also appears to decay slowly during annealing, when we observe only "normal" Ostwald ripening. Thus wetting layer consumption cannot explain the novel coarsening kinetics observed during deposition.

Island faceting might generally be expected to slow down coarsening kinetics, but since faceting does not change during growth or annealing, this cannot explain our results.

Previous experiments have shown that, for Ge-rich coherent islands, interdiffusion between the islands and the Si substrate can occur [23]. If interdiffusion were important we would expect it to affect coarsening during static annealing. But, again, our static annealing experiments exhibit normal coarsening kinetics, even though the anneal is performed at the same temperature as deposition, and the duration of the anneal significantly exceeds the total deposition time. Thus we also reject interdiffusion as the cause of the coarsening kinetics observed during growth.

Another possible mechanism for coarsening is static coalescence [15], which is almost certainly occurring within our dense island arrays. The kinetics of coarsening due to liquidlike coalescence during deposition have been derived by Beysens *et al.* and by Family and Meakin (FM) [12,24]. Using statistical self-similarity arguments, FM showed that for 3D islands growing in a 2D diffusion field, $\langle V(t)\rangle \propto t^3$, which is consistent with our experimental results. Unfortunately, the time dependence of $\langle N(t)\rangle$ resulting from coalescence cannot be determined from self-similarity [24], so we cannot discriminate quantitatively to what degree coalescence contributes to the overall kinetics of coarsening.

In summary, using real-time light scattering during deposition we observed novel coarsening kinetics in dense arrays of hut clusters. Ostwald ripening is enhanced by elastic repulsion energy between the islands, coupled with deposition that forces the islands closer together, thereby driving up the system energy. A three-dimensional analog to the system described here would be the coarsening of coherently strained precipitates from solid solution, where coarsening and precipitation occur simultaneously. Elastic repulsion effects would be important only for a high volumetric density of precipitates, and have not been observed to our knowledge.

We express our gratitude to Peter Voorhees, Jerry Tersoff, and Corbett Bataille for useful discussions, John Hunter for technical assistance, and Bonnie McKenzie for SEM. L. B. F. acknowledges the MRSEC program at Brown University funded by the National Science Foundation under Award No. DMR-9632524. Sandia is a multiprogram laboratory operated by Sandia Corporation, a Lockheed Martin Company, for the United States Department of Energy under Contract No. DE-AC04-94AL85000.

*Electronic address: jafloro@sandia.gov

[1] Y.-W. Mo, D. E. Savage, B. S. Swartzentruber, and M. G. Lagally, Phys. Rev. Lett. **65**, 1020 (1990).
[2] D. J. Eaglesham and M. Cerullo, Phys. Rev. Lett. **64**, 1943 (1990).
[3] S. Guha, A. Madhukar, and K. C. Rajkumar, Appl. Phys. Lett. **57**, 2110 (1990).
[4] D. E. Jesson, K. M. Chen, S. J. Pennycook, T. Thundat, and R. J. Warmack, Science **268**, 1161 (1995).
[5] J. Tersoff and F. K. LeGoues, Phys. Rev. Lett. **72**, 3570 (1994).
[6] G. Springholz, V. Holy, M. Pinczolits, and G. Bauer, Science **282**, 734 (1998).
[7] Jian-hong Zhou, K. Brunner, G. Abstreiter, O. Kienzle, and F. Ernst, Thin Solid Films **336**, 252 (1998).
[8] J. A. Floro, E. Chason, M. B. Sinclair, L. B. Freund, and G. A. Lucadamo, Appl. Phys. Lett. **73**, 951 (1998).
[9] I. M. Lifshitz and V. V. Slyozov, J. Phys. Chem. Solids **19**, 35 (1961).
[10] B. K. Chakraverty, J. Phys. Chem. Solids **28**, 2401 (1967).
[11] L. Bardotti, M. C. Bartelt, C. J. Jenks, C. R. Stoldt, J. M. Wen, C. M. Zhang, P. A. Thiel, and J. W. Evans, Langmuir **14**, 1487 (1998).
[12] D. Beysens, C. M. Knobler, and H. Schaffar, Phys. Rev. B **41**, 9814 (1990).
[13] F. M. Ross, J. Tersoff, and R. M. Tromp, Phys. Rev. Lett. **80**, 984 (1998).
[14] G. Medeiros-Ribiero, T. I. Kamins, D. A. A. Ohlberg, and R. Stanley Williams, Phys. Rev. B **58**, 3533 (1998).
[15] N. Pinto, R. Murri, and R. Rinaldi, Thin Solid Films **336**, 53 (1998).
[16] J. A. Floro, E. Chason, L. B. Freund, R. D. Twesten, R. Q. Hwang, and G. A. Lucadamo, Phys. Rev. B **59**, 1990 (1999).
[17] E. Chason, M. B. Sinclair, J. A. Floro, J. A. Hunter, and R. Q. Hwang, Appl. Phys. Lett. **72**, 3276 (1998).
[18] J. A. Floro, E. Chason, R. D. Twesten, R. Q. Hwang, and L. B. Freund, Phys. Rev. Lett. **79**, 3946 (1997).
[19] J. A. Floro and C. V. Thompson, Acta. Metall. Mater. **41**, 1137 (1993).
[20] J. A. Floro, G. A. Lucadamo, E. Chason, L. B. Freund, M. Sinclair, R. D. Twesten, and R. Q. Hwang, Phys. Rev. Lett. **80**, 4717 (1998).
[21] For this value of Φ, the supersaturation from the flux is about equal to the supersaturation due to capillarity.
[22] G. Medeiros-Ribeiro, T. I. Kamins, D. A. A. Ohlberg, and R. Stanley Williams, Phys. Rev. B **58**, 3533 (1998).
[23] S. A. Chaparro, Jeff Drucker, Y. Zhang, D. Chandrasekhar, M. R. McCartney, and David J. Smith, Phys. Rev. Lett. **83**, 1199 (1999).
[24] Fereydoon Family and Paul Meakin, Phys. Rev. Lett. **61**, 428 (1988).